Laboratory Investigation (2019) 99:1470–1483
https://doi.org/10.1038/s41374-019-0266-1

ARTICLE

A phosphorylation-deficient mutant of retinoid X receptor α at Thr 167 alters fasting response and energy metabolism in mice

Tatsuya Sueyoshi[1] · Tsutomu Sakuma[1] · Sawako Shindo[1] · Muluneh Fashe[1] · Tomohiko Kanayama[1] · Manas Ray[2] · Rick Moore[1] · Masahiko Negishi[1]

Received: 11 December 2018 / Revised: 14 April 2019 / Accepted: 29 April 2019 / Published online: 31 May 2019

Abstract

Retinoid X receptor α (RXRα) has a conserved phosphorylation motif at threonine 162 (humans) and threonine 167 (mice) within the DNA-binding domain. Here we have generated RXRα knock-in mice (*Rxrα*^{T167A}) bearing a single mutation of Thr 167 to alanine and examined the roles of Thr 167 in the regulation of energy metabolism within adipose, muscle, and liver tissues. *Rxrα*^{T167A} mice exhibited down-regulation of metabolic pathways converting glucose to fatty acids, such as acetyl-CoA carboxylase in the white adipose tissue (WAT) and ATP citrate lyase in the muscle. They also reduced gene expression for genes related to fatty acid catabolism and triglyceride synthesis in WAT and controlled heat factors such as adrenergic receptor β1 in muscles. In contrast, hepatic gluconeogenic pathways and synthetic pathways related to fatty acids remained unaffected by this mutation. Expression of multiple genes that were affected by the Thr 167 mutation in adipose tissue exhibited clear response to LG100268, a synthetic RXR agonist. Thus, the altered gene expression in mutant mice adipose appeared to be a direct effect of RXRα Thr 167 mutation and by some secondary effect of the mutation. Blood glucose levels remained normal in *Rxrα*^{T167A} during feeding, as observed with RXRα wild-type mice. However, *Rxrα*^{T167A} mice exhibited an attenuated decrease of blood glucose levels that occurred after fasting. This attenuation correlated with a concomitant down-regulation of lipid metabolism in WAT and was associated with RXRα phosphorylation at Thr 167. Thus, Thr 167 enabled RXRα to coordinate these three organs for regulation of energy metabolism and maintenance of glucose homeostasis.

Introduction

Members of the nuclear receptor superfamily conserve a phosphorylation motif between the two zinc fingers of their DNA-binding domains (DBDs). This motif is conserved in 41 of the total 46 human nuclear receptors, and their corresponding mouse nuclear receptors. This extremely high cross-species conservation suggests the possibility that this phosphorylation functions as a general regulator for nuclear receptor function. Phosphorylation of this motif was first reported with constitutive active/androstane receptor (CAR, NR1I3) at threonine 38 in mouse liver [1, 2]. Dephosphorylation in the cytoplasm activates CAR and elicits a translocation to the nucleus, while phosphorylation in the nucleus inactivates CAR and expels it from the nucleus [1–3]. Similarly, the mouse farnesoid X receptor (FXR, NR1H4), which contains this motif at serine 154, was found to be phosphorylated in the nucleus of hepatocytes [4]. Phosphorylation of serine 154 occurred following ligand activation to inactivate FXR, thus linking ligand activation and accelerated degradation/inactivation. Mouse estrogen receptor α (ERα, NR3A1) is specifically phosphorylated at serine 216 in only immune cells such as neutrophils and macrophages [5, 6]. Analyses of ERα S216A KI mice that bear a single mutation of serine 216 to alanine revealed that phosphorylated ERα exerts

Supplementary information The online version of this article (https://doi.org/10.1038/s41374-019-0266-1) contains supplementary material, which is available to authorized users.

✉ Tatsuya Sueyoshi
Sueyoshi@niehs.nih.gov

[1] Pharmacogenetics section, Reproductive and Developmental Biology Laboratory, National Institute of Environmental Health Sciences, National Institutes of Health, Research Triangle Park, NC 27709, USA

[2] Knockout Mouse Core, National Institute of Environmental Health Sciences, National Institutes of Health Research, Triangle Park, NC 27709, USA

anti-inflammatory and anti-apoptotic functions in mice (Sawako Shindo, Shih-Heng Chen, Saki Gotoh, Manas Ray, Rick Moore, Jennifer Martinez, John Hong, Masahiko Negishi, unpublished data). In addition, although their phosphorylation has not yet been confirmed in tissues in vivo, cell-based mutation studies suggest that numerous other nuclear receptors can also be regulated through this conserved motif [4, 7, 8]. Thus, this conserved phosphorylation motif provides a target for investigations to explore the actions and regulations of nuclear receptors, and to integrate their diverse biological functions with other cell signaling systems.

Retinoid X receptor α (RXRα, NR2B1) contains this conserved motif at threonine 167. RXRα, a unique member of the nuclear receptor superfamily, engages in widespread and diverse functions to regulate physiological and pathophysiological processes, as well as pharmacological responses, by forming heterodimers with numerous other nuclear receptors [9–12]. In general, activation and specificity of RXRα functions are understood as coming from these heterodimer partners. Although ligand activators such as 9 *cis*-retinoic acid for RXRα are known, whether they, in fact, regulate any biological functionalities of RXRα remains unexplored. Recently, RXRα was found to be phosphorylated at serine 260 in Ras-transformed keratinocytes and to repress vitamin D receptor (VDR) activity by regulating their intracellular localization [13]. Here, our study focused on threonine 167 to understand how this phosphorylation enables RXRα to regulate activities of its heterodimer partners. Moreover, we generated and utilized RXRα knock-in (KI) mice (RXRα T167A KI or $Rxr\alpha^{T167A}$) bearing a single mutation of threonine 167 to alanine to evaluate the functionality of this phosphorylation in vivo.

Materials and methods

Plasmids

Human RXRα full-length complementary DNA (cDNA) was cloned into pcDNA3.1 with a 3× Flag™ Tag at the N terminus of the protein sequence. Here, Thr 162 codon (ACG) was mutated to codons for Ala (GCG) or Asp (GAC) using the QuickChange mutagenesis system (Stratagene). cDNAs for human peroxisome proliferator-activated receptor α (PPARα), PPARγ, and VDR, were cloned into pcDNA3.1. Glutathione *S*-transferase human RXRα expression vector for *Escherichia coli* was constructed with pGEX4T-3. CAR/pCR3, PXR/pCR3, and NR1x5 (luciferase reporter for CAR) were previously reported [14–16]. PPRE luciferase reporter was kindly provided by Dr. Frank Gonzalez [17]. Protein kinase Cα (PKCα) CAT was a gift from Bernard Weinstein (Addgene plasmid # 21234) [18].

Antibody development

A polyclonal antibody against anti-phospho-Thr 167 peptide of RXRα (anti-p-Thr 167 RXRα) was produced and evaluated by GenScript (Piscataway, NJ, USA). The peptide sequence used for immunizing rabbits was CKGFFKR-pT-VRKDLTY ("pT" indicates phosphorylated Thr).

In vitro PKC phosphorylation

RXRα was expressed as a glutathione *S*-transferase fusion protein in *E. coli* and purified as described previously [1]. The hRXRα protein moiety was eluted by thrombin cleavage from the fusion protein bound to GSH Sepharose. In vitro PKC phosphorylation reaction was performed as previously reported [1], and phosphorylation at Thr 167 was detected by western blotting using anti-p-Thr 167 RXRα antibody.

Cell culture

Huh7 and COS-1 cells were cultured in Dulbecco's modified Eagle's medium and U87 human glioblastoma cell line was cultured in minimum essential medium at 37 °C in a humidified atmosphere containing 5% CO_2. Media were supplemented with 10% fetal bovine serum, 100 U/mL penicillin, and 100 g/mL streptomycin. FuGENE 6 was used to transfect cells with expression and reporter plasmids.

Electrophoretic mobility shift assay

Electrophoretic gel mobility shift assays were performed as described in previous reports [19]. The DNA probes used were GATCAAAACTAGGTCAAAGGTCA and GATCT GACCTTTGACCTAGTTTT for PPARα and PPARγ [20]; GATCTCTGTACTTTCCTGACCTTG and GATCCAAG GTCAGGAAAGTACAGA for CAR [16]; GATCCCGGA CGCCCTCGCTCACCTCGCTGA and GATCTCAGCG AGGTGAGCGAGGGCGTCCGG for VDR [21]; and GAT CATATGAACTCAAAGGAGGTCAGTG and GATCCAC TGACCTCCTTTGAGTTCATAT for PXR [22]. Annealed double-strand DNA was labeled with ^{32}P dATP by fill-in reaction using DNA polymerase Klenow fragments. Each protein factor was produced using in vitro transcription/translation reactions performed with TnT T7 Quick Coupled Transcription/Translation System (Promega). Labeled DNA and protein complexes were separated on 4% acrylamide gels in electrophoresis buffer (7 mM Tris-HCl (pH 7.5), 3 mM sodium acetate, and 1 mM EDTA). DNA protein complexes were formed in 10 µL reaction containing 0.5 µL each of in vitro translated proteins, labeled oligonucleotides

(30,000 cpm), 0.05% NP40, 10% glycerol in 5 mM Tris-HCl (pH 7.5), 25 mM NaCl, 250 μM dithiothreitol buffer at room temperature. Dried gels were exposed against autoradiography films to visualize mobility shifted bands.

Reporter assay

Huh7 or COS-1 cells were co-transfected with expression vectors for RXRα mutants with their heterodimer partners for respective luciferase reporters. The reporters used were PPRE-Luc [17] and NR1x5 Luc (for CAR) [15]. Twenty-four hours after transfection each ligand shown in the figure legends were added into the cell culture media. After the 24 h induction period, luciferase activities were determined with the Dual Luciferase Assay System (Promega) and presented with the results of firefly luciferase activities normalized to Renilla luciferase activities.

Liver in vivo expression of YFP-tagged RXRα

Yellow fluorescent protein (YFP)-tagged hRXRα expression and visualization in confocal microscope was performed as described in previous reports [1]. YFP-hRXRα, YFP-hRXRα T162A, or YFP-hRXRα T162D expression vectors were injected into mouse blood stream through the tail vain using TransIt Gene Delivery System (Mirus). Eight hours after the procedure, mice were sacrificed, and liver frozen sections were prepared. Microscope images were captured with a Zeiss LSM 510 confocal scanning microscope. Localization of these RXRα fusion proteins were analyzed as described in previous publications [1].

RXRα T167A KI (*Rxra*^{T167A}) mice

Mouse genomic DNA containing introns 1–4 (including exons 2, 3, and 4) was PCR amplified using LA *Taq* polymerase (Takara). Cloned genomic DNA was used as a template for site-directed mutagenesis to introduce Thr 167 to Ala mutation in exon 4. The 5.7 kb left arm including exons 2, 3, and 4 plus 2.6 kb right arm containing a part of intron 4 was cloned into a targeting vector with two multi-cloning sites, ACN cassette and DT-A cassette. Linearized targeting vector was transfected via electroporation into C57B/6 ES cells. ES clones resistant to G418 were screened by PCR and by Southern blotting. The heterozygous ES clones were injected into C57BL/6 blastocysts. Obtained chimera male mice were used for establishing germline transmission. Confirmed heterozygous mice were interbred to obtain homozygous wild-type (WT) and T167A mutant mice. Genotypes of these mice were determined by PCR amplifications designed to amplify the mutation area. The results in this report were obtained with these homozygous WT and mutant mice.

Animal treatments

All animals were housed in a room maintained at 22 °C with a 12:12-h light/dark cycle (7:00 a.m. to 7:00 p.m.). Mice were fed ad libitum with NIH-31 Open Formula Autoclavable diet (Zeigler). WT and T167A mutant mice (14–16 weeks old, $n = 4$) fed and fasted (24 h food withdrawn) were sacrificed for RNA and protein preparations. RXR agonist LG100268 (30 mg/kg) was administered as a single oral dose to WT and T167A mutant mice via gavage using corn oil (200 μL/mouse) and then mice were kept in fed and fasted conditions for 24 h. All animal procedures were approved by the Animal Care and Use Committee at NIEHS, NIH, and performed humanely in accordance with the Public Health Service Policy.

Gene array analysis

Messenger RNA (mRNA) from adipose, liver, and muscle was purified using Trizol reagent and RNeasy mini kit using WT-fed, WT-fasted, KI-fed, and KI-fasted groups ($n = 4$). Gene expression analysis was conducted using Agilent Whole Mouse Genome 4 × 44 multiplex format oligo arrays (014868) (Agilent Technologies) following the Agilent 1-color microarray-based gene expression analysis protocol. Starting with 500 ng of total RNA, Cy3-labeled cRNA was produced according to the manufacturer's protocol. For each sample, 1.65 μg of Cy3-labeled cRNAs were fragmented and hybridized for 17 h in a rotating hybridization oven. Slides were washed and then scanned with an Agilent Scanner. Data were obtained using the Agilent Feature Extraction software (v12), using the 1-color defaults for all parameters. The Agilent Feature Extraction Software performed error modeling, adjusting for additive and multiplicative noise. The resulting data were processed using the OmicSoft Array Studio (Version 9.0) software. Gene expression comparisons among obtained datasets were performed with the Ingenuity Pathway Analysis software (Qiagen). Threshold for gene expression changes were set to >5-fold and $P < 0.05$ and >2-fold and $P < 0.05$.

Quantitative RT-PCR analysis of mRNA

Total RNA of each tissue was isolated with Trizol reagent (Invitrogen). Reverse-transcription was performed with High Capacity cDNA Archive kit for RNA (Applied Biosystems). CFX96 Real Time System (Bio-Rad) was used for quantitative PCR (qPCR) reaction. Taqman probes and primers used are listed in Supplemental data section. *Actb* gene expression determined with TaqMan mouse ACTB endogenous control reagent (Applied Biosystems) was used for normalization of gene expression among individual mice.

Western blotting

Protein from adipose tissue was extracted as previously described [23] and mouse liver nuclear extracts was prepared as in [19]. Protein extract concentration was determined using Bio-Rad protein assay. Proteins were separated on a sodium dodecyl sulfate-polyacrylamide gel electrophoresis and electro-transferred to a polyvinylidene fluoride membrane. The membrane was incubated in 5% skim milk in 50 mM Tris-HCl (pH 7.5), 0.1 M NaCl, and 0.05% Tween-20 for 1 h at room temperature. Phosphorylated RXRα was detected with anti-p-Thr 167 RXRα antibody diluted in 5% bovine serum albumin by incubating overnight at 4 °C. Washed membrane was incubated with secondary antibody (horse radish peroxidase-conjugated anti rabbit IgG) and positive bands were visualized with WesternBright Sirius chemiluminescent reagents (Advansta) and recorded with a western blot scanner (Licor). For detecting transfected flag-tagged RXRα in cultured cell line, anti-Flag antibody was used.

Statistical analysis

Multiple groups were analyzed by one-way analysis of variance followed by Tukey's multiple comparison test. Two groups were compared by Student's *t* test. These statistical analyses were conducted using the software GraphPad Prism.

Results

RXRα phospho-mimetic mutation differentially affects DNA interactions of RXRα heterodimers

Threonine 162 in the PKC recognition motif of RXRα DBD is highly conserved among nuclear receptors, as shown in several examples within Fig. 1a. We have constructed plasmids expressing human RXRα with mutated Thr 162 to Ala (to mimic the non-phosphorylated form) and Asp (to mimic the phosphorylated form).

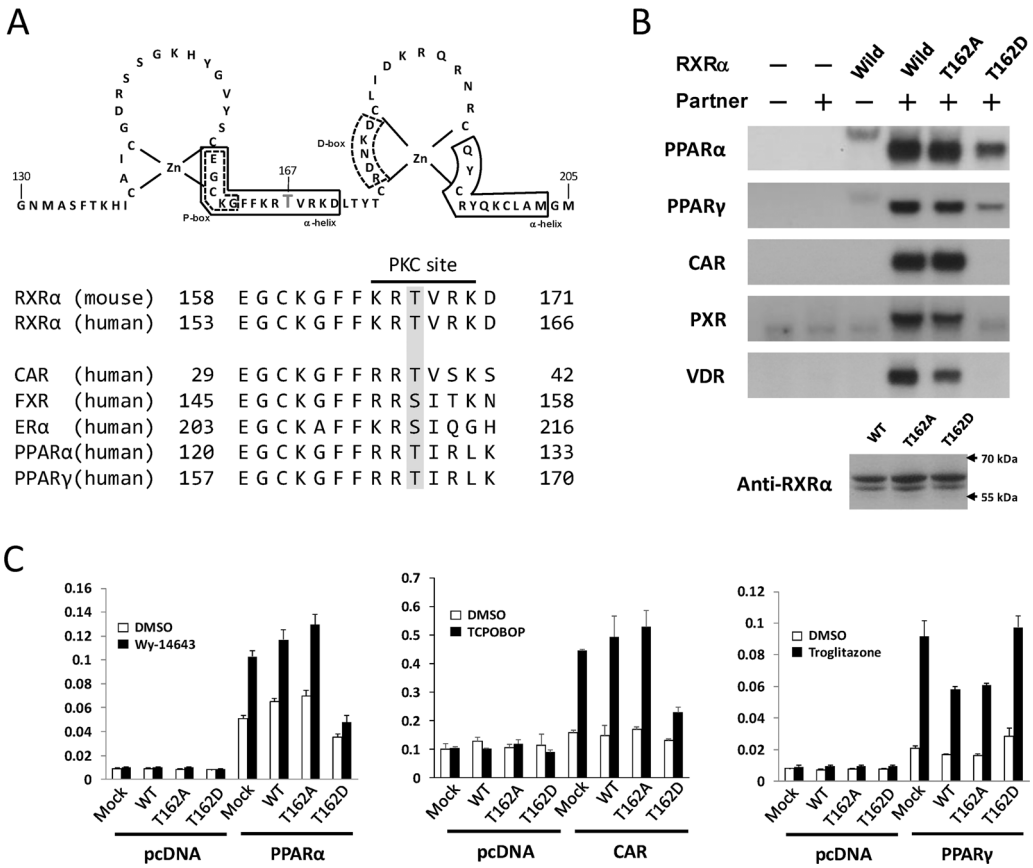

Fig. 1 Phospho-mimetic mutation of retinoid X receptor α (RXRα) affects its activity partner dependently. **a** Conserved phosphorylation sites in DNA-binding domains of selected nuclear receptors. **b** Partner-dependent effect of phospho-mimetic mutation of RXRα in electrophoretic mobility shift assay. Each nuclear receptor protein was produced by in vitro translation. ^{32}P-labeled double-strand oligo probe for each heterodimer complex was mixed with the proteins and separated on polyacrylamide gels. Only mobility shifted bands are shown here. As a control experiment, wild-type (WT) and mutant RXRα protein expression was detected by western blotting and shown at the bottom. **c** Partner-dependent effect of RXRα phospho-mimetic mutant in gene reporter assay. Luciferase reporter assays were performed as described in Materials and methods. Values on vertical axes indicate normalized firefly luciferase activities. For each receptor, ligand-treated activities are shown with black bars

Utilizing in vitro translated RXRα mutants with RXRα heterodimer partners PPARα, PPARγ, CAR, PXR, and VDR, gel shift analyses were performed to model the effects of Thr 162 phosphorylation state on heterodimer DNA-binding ability (Fig. 1b). When coupled to the T162D mutant, CAR, PXR, and VDR completely lost their DNA interaction abilities to each prototype DNA element probe. In contrast, heterodimers with PPARα and PPARγ retained their DNA-binding activity with T162D, albeit with lower activities compared with T162A mutant. These results suggested that phosphorylation at Thr 162 has different effects across nuclear receptors, depending on which partner is involved in a given gene regulation process. We next examined the ability of these mutants to facilitate CAR, PPARα, and PPARγ activity in a gene reporter assay (Fig. 1c). Except in the case of PPARγ, T162D mutation within RXRα in heterodimers with PPARα or CAR shows attenuated gene reporter activity when compared to WT or T162A mutant. However, with PPARγ-RXRα T162D, heterodimer activation was stronger than WT or T162A. Thus, the outcome of the phosphorylation of RXRα in target gene regulation appears to be diverse and depends on which partner is playing the major role for transcriptional regulation.

Phosphorylation of RXRα Thr 162

Bacterially expressed RXRα was phosphorylated by in vitro incubation with PKC (Fig. 2a, left panel), as clearly indicated by the western blotting with anti-p-Thr 167 RXRα-specific antibody in WT, but not T162A mutant. Furthermore, co-transfection of Huh7 cells with RXRα and active PKC expression vectors replicated the results of Thr 162 phosphorylation (Fig. 2a, right panel). Without kinase co-transfection in U87 cells, Thr 162 was phosphorylated as shown in Fig. 2b. U87 cells were transfected with either WT RXRα or T162A expression vector. Whole-cell extracts of

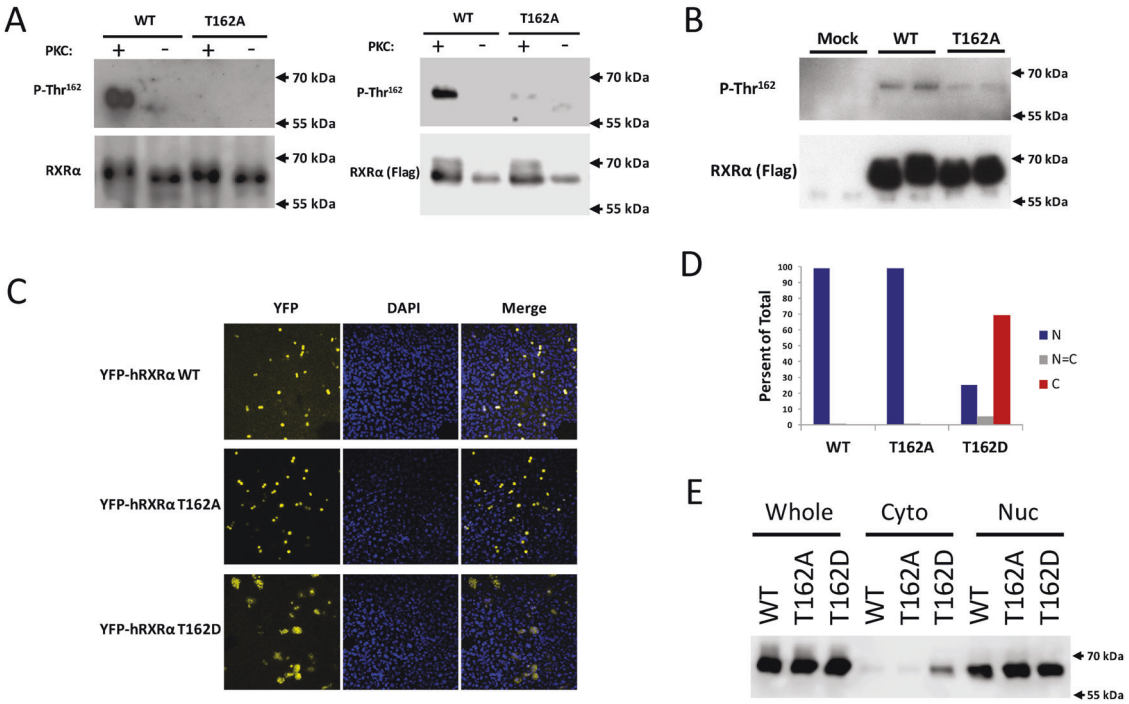

Fig. 2 Retinoid X receptor α (RXRα) phosphorylation and subcellular localization. **a**, Left panel: Bacterially expressed RXRα was phosphorylated by protein kinase C (PKC). Phosphorylated RXRα was detected by western blotting with a phospho-specific antibody (P-Thr 167). Anti-RXRα western blotting was also performed as a control. Right panel: Ectopically expressed RXRα in Huh7 cells was phosphorylated by PKC. Huh7 cells were co-transfected with Flag-tagged RXRα and PKC catalytic domain expression vectors. Whole-cell extract was subjected to western blotting with P-Thr 167 and anti-Flag antibodies. **b** Ectopically expressed RXRα in U87 cells were phosphorylated at T167 without kinase transfection. U87 human glioblastoma cells were transfected with an RXRα expression vector and whole-cell extracts were subjected to western blotting with P-Thr 167 and anti-Flag antibodies. **c** Phospho-mimetic mutation affected RXRα subcellular localization. YFP-hRXRα WT, YFP-hRXRα T162A, and YFP-hRXRα T162D proteins were expressed in mouse liver and their subcellular localizations were analyzed by confocal microscopy. **d** YFP-hRXRα fusion protein localizations in **c** results were categorized into three groups. Blue, gray, and red bars show predominantly in nucleus, equal distribution between nucleus and cytoplasm, and predominantly in cytoplasm, respectively. **e** Ectopically expressed RXRα localization in Huh7 cells. Nuclear and cytoplasmic extracts were subjected to western blotting analysis using anti-RXRα antibody

transfected U87 were analyzed by western blotting with an anti-p-Thr 167 RXRα antibody, and the results suggested that RXRα was phosphorylated in U87 cells by unidentified kinases.

Intracellular localization of phosphorylated RXRα

We constructed YFP-tagged RXRα and its mutant to visualize localization changes caused by phospho-mimetic mutations. YFP-RXRα WT, YFP-RXRα T162A (non-phospho-mimetic mutant) and YFP-RXRα T162D (phospho-mimetic mutant) were expressed in mouse liver and visualized as shown in Fig. 2c, d and Supplemental Fig. 1. Both WT and the T162A mutant were exclusively localized in the nucleus. In contrast, mutation to aspartic acid dramatically changed localization. Nearly 100% of WT and T162A localized in the nucleus, while approximately 70% of hepatocytes expressing the T162D mutant showed cytoplasmic localization. In the cultured Huh7 cell line, T162D increased cytoplasmic localization of RXRα in western blotting analysis (Fig. 2e). Combined, these results suggested that Thr 162 phosphorylation may regulate RXRα nucleo-cytoplasmic localization.

RXRα T167A KI (*Rxrα*^{T167A}) mice

To further analyze biological functions of RXRα T167 phosphorylation, we have established a mouse line with a single mutation of threonine 167 to alanine in the RXRα gene (Fig. 3a, b). Homologous recombination was confirmed by hybridization with a 5′ and 3′ probe using *Bgl*II- and *Bam*HI-digested genomic DNA, respectively (Fig. 3c). Hybridization with a 5′ probe using *Bgl*II-digested genomic DNA gave 14.4 and 11.5 kb bands as expected when the designed recombination was introduced. Southern blotting with a 3′ probe using *Bam*HI-digested DNA produced 9 and 5.9 kb fragments (Fig. 3c). The targeted genome site in mice was confirmed by PCR amplification (Fig. 3d), and mutation of mRNA was detected by cDNA sequencing. Introduction of this mutation barely affected RXRα mRNA and protein expression levels in liver cell nuclei (Fig. 3e). Both T167A KI females and males were fertile.

Gene expression comparison between WT and T167A KI mice

We observed varied effects of phospho-mimetic mutation of RXRα on DNA-binding and gene reporter assays,

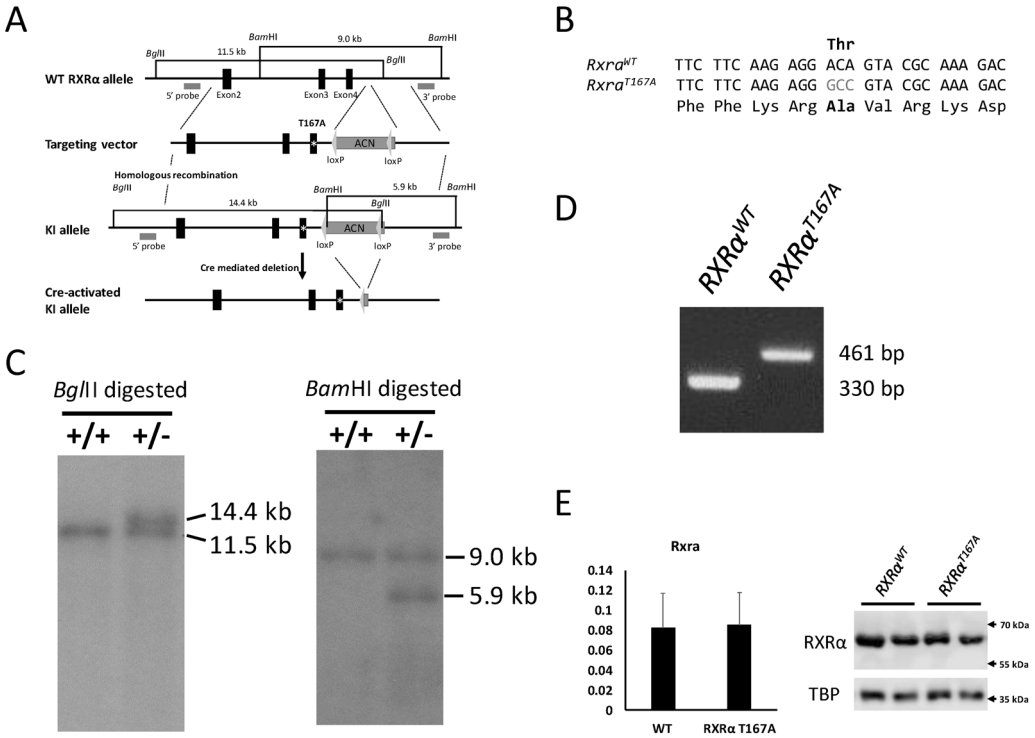

Fig. 3 Retinoid X receptor α (RXRα) T167A KI (*Rxrα*^{T167A}) mice. **a** Schematic diagram showing strategy for producing *Rxrα*^{T167A} mice. **b** Targeted codon sequence. **c** Southern blotting of wild-type (WT) and homologous DNA recombination-positive ES cells using 5′ probe (left) and 3′ probe (right). **d** PCR amplification of genomic DNA fragments including mutated area from WT and *Rxrα*^{T167A} mice. **e** RXRα messenger RNA (mRNA) in the liver (left panel) and RXRα protein in liver nuclear extracts (right panel) from WT and *Rxrα*^{T167A} mice were determined by quantitative PCR (qPCR) analysis and western blotting, respectively. Vertical axes indicate the relative amount of RXRα mRNA vs. that of β-actin mRNA. TBP stands for TATA-binding protein used for loading control

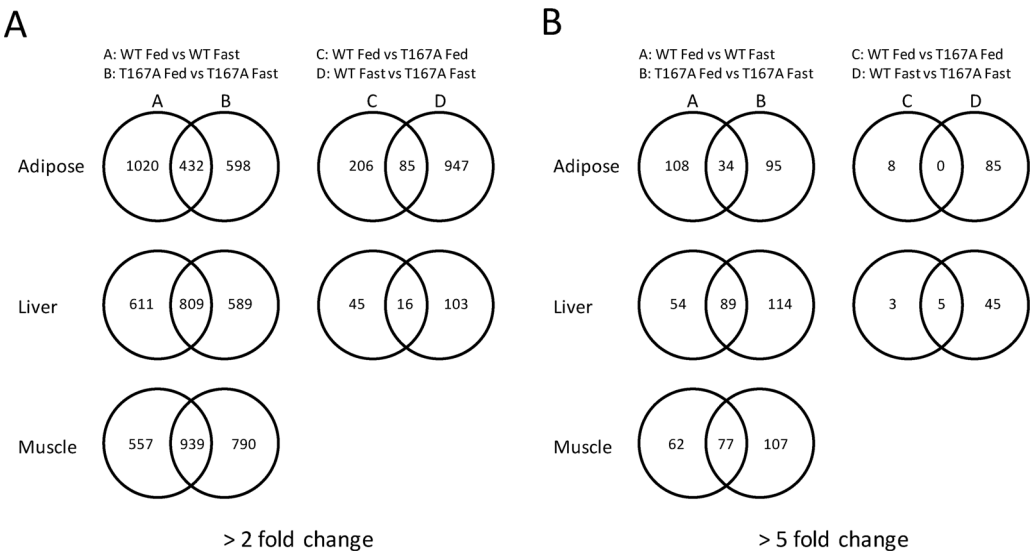

Fig. 4 Gene expression changes in $Rxr\alpha^{T167A}$ mice. Venn diagram using DNA microarray data from wild-type (WT) and $Rxr\alpha^{T167A}$ mice in fed and fasted conditions. Microarray analyses were performed using adipose, liver, and muscle messenger RNA (mRNA) as described in Materials and methods. **a** Venn diagram using dataset with 2-fold gene expression change threshold ($P < 0.05$). **b** Venn diagram using dataset with 5-fold gene expression change threshold ($P < 0.05$)

Table 1 Gene numbers affected by fasting in WT and RXRα T167A mice

	WT or T167A specific	Common	Ratio (specific/common)
2-fold change			
Adipose	1020 + 598 = 1618	432	3.75
Liver	611 + 589 = 1200	809	1.48
Muscle	557 + 790 = 1347	939	1.43
5-fold change			
Adipose	108 + 95 = 203	34	5.97
Liver	54 + 114 = 168	89	1.89
Muscle	62 + 107 = 169	77	2.19

Gene numbers were counted on the data presented in Fig. 4 Venn diagrams

WT wild type, *RXRα* retinoid X receptor α

depending on the heterodimer (Fig. 1b, c). Since RXRα is ubiquitously expressed and each organ has diverse collections and expression levels of RXRα heterodimer partners, phosphorylation may affect the expression of numerous genes in an unpredictable manner over a myriad of biological processes. Here, we performed gene microarray analysis using WT and T167A KI mice in fed and fasting conditions. We focused on three tissues (white adipose, liver, and muscle) where RXRα and PPARs play major roles in gene regulation. In Supplemental Fig. 2, body weight, liver weight, white adipose weight, and blood chemistry data obtained from mice used in the microarray study are shown. The results indicated no apparent differences in these parameters between WT and T167A KI mice.

The Venn diagrams of the microarray results using two datasets with different thresholds (2-fold change with $P < 0.05$, or 5-fold change with $P < 0.05$) are presented in Fig. 4. One set of Venn diagrams used data comparison A: WT fed vs. WT fasted and B: T167A fed vs. T167A fasted (AB diagram) and the other set used C: WT fed vs. T167A fed and D: WT fasted vs. T167A fasted (CD diagram). The AB diagram suggested fasting caused more genes to be specifically regulated in either WT or T167A mice compared to commonly regulated genes as summarized in Table 1 for all these organs (e.g., in adipose: $1020 + 598 > 432$ (2-fold threshold), $108 + 95 > 34$ (5-fold threshold)). Thus, the results suggested that the RXRα T167A mutation caused fasting response changes in these organs. Furthermore, the CD diagrams again indicated that fasting divergently altered gene expression of WT and T167A mice in the adipose and liver. In fed conditions, a smaller number of genes (adipose: 206; liver: 45) showed more than 2-fold differences in expression, while a much larger number of genes (adipose: 947; liver: 103) exhibited differential expression in fasting conditions. In the 5-fold threshold dataset, the same type of differential expression was observed (adipose: 8; liver: 3 vs. adipose: 85, liver 45). These results suggested that the difference between WT and $Rxr\alpha^{T167A}$ became more profound under fasting condition in these organs. In muscle, no significantly different gene expression was observed between WT fed vs. T167A KI fed or WT fasted vs. T167A KI fasted.

We compared the ratio between specifically regulated genes vs. commonly regulated genes by fasting in WT and $Rxr\alpha^{T167A}$ adipose, liver, and muscle as presented in

Table 1. Since both WT and T167A mutant-specific gene expression observed in these Venn diagrams were caused by the T167A mutation, this specific/common ratio are considered as the scale of impact on gene expression caused by this mutation. Among these three tissues, adipose displays the highest ratio of specific gene expression changes in the 2-fold and 5-fold threshold conditions, suggesting that the T167A mutation has most pronounced effects on fasting responses in adipose tissue. Moreover 5.97 (5-fold threshold) and 3.75 (2-fold threshold) adipose-specific/common ratios suggested genes affected more strongly by fasting have a greater predisposition to be affected by the T167A mutation.

Next, we focused on determining the mutation effect on fasting-induced changes of the canonical biological pathways in these mice. Thus, we utilized Ingenuity Pathway Analysis for WT and $Rxr\alpha^{T167A}$ adipose, liver, and muscle tissue datasets and the affected canonical pathways found were listed in Supplement Tables 1, 2, and 3. In adipose, 62 canonical pathways in the WT dataset and 85 pathways in the $Rxr\alpha^{T167A}$ dataset were significantly altered ($P < 0.05$) by fasting. Only 31 pathways overlapped between these altered ones, suggesting that the Thr 167 mutation caused significantly divergent fasting changes for canonical pathways in these mice adipose tissues. The heat map shown in Fig. 5a also suggests a very strong divergent response in canonical pathways between the two strains in the adipose. In liver, 73 and 85 pathways were affected in WT and $Rxr\alpha^{T167A}$, respectively, and 54 of them overlapped. It appeared that the genotype-dependent fasting effect was less severe in the liver compared to the adipose. In the muscle, 33 and 30 pathways were affected for the same mice. Fewer pathways were affected by fasting and the $-\log(P$ value) for these pathway changes were much smaller in the muscle compared with the other two organs. Only 12 of them were overlapped.

For a clear illustration of specific pathway alteration in adipose, we limited canonical pathway analyses on pathways related to lipid metabolism and to RXRα functions, then the obtained $-\log(P$ value)s were plotted in Fig. 5b. While RXRα-related canonical pathways were differentially affected by fasting between WT and mutant mice (e.g., LXR/RXR activation $-\log(P$ value)s in WT and $Rxr\alpha^{T167A}$ were 1.52 and 10.17, respectively), most metabolic pathways were similarly affected (e.g., triacylglycerol biosynthesis $-\log(P$ value)s in WT and $Rxr\alpha^{T167A}$ were 3.62 and 3.41, respectively). Even for this very similar $-\log(P$ value)s for the triacylglycerol biosynthesis pathway, the array data showed differential regulation of *Dgat2* and *Gpam* in this pathway between WT and $Rxr\alpha^{T167A}$. These gene expression differences may be reflected in *Z*-score differences in the triacylglycerol biosynthesis pathway (WT = −0.632 vs. $Rxr\alpha^{T167A}$ = −1.414). In the LXR/RXRα activation pathway, Acc1 differential regulation was observed. We confirmed the differential expression of all three genes in Fig. 5c by qPCR analysis. Furthermore, the 5-fold threshold Venn diagram in Fig. 4b suggested *Acsm3*, *Mogat2*, and *Prkag3* differential expression and qPCR confirmed significant different expression of these genes (Fig. 5c). Similar analyses found differentially regulated candidate genes in the liver and muscle. qPCR analysis results of these genes are presented in Fig. 5d (*Igf2*, *Saa1*, and *Slc3a1* in the liver and *Acly*, *Adrb1*, and *Ppp1r3b* in the muscle). Most of these genes are thought to be directly or indirectly involved in energy metabolism.

Thr 167 to Ala mutation attenuated blood glucose decrease by fasting

We measured blood glucose levels in mice used in the gene expression array study in Fig. 4 and presented in Fig. 6a. In WT mice, glucose levels were lower after 24 h food withdrawal, as expected. In contrast, no significant decrease in blood glucose was observed after the same period of fasting in T167A mice. Next, we measured mRNA expression levels of canonical energy metabolizing enzymes in the liver (Fig. 6b). The examined genes were *G6pc*, *Pck1* (gluconeogenesis), *Acc1*, *Fasn*, *Scd1* (fatty acid synthesis), *Hmgcs2*, *Cpt1a* (β-oxidation of fatty acid), and *Pparα* (a key transcription factor of energy metabolism in liver). Results showed no clear difference in these gene targets between WT and T167A mice, regardless of fed or fasting conditions.

We next focused on adipose tissue, since we observed many energy-metabolizing enzyme gene expression changes in the microarray study (Fig. 5c). We performed western blotting analysis of adipose tissue extracts as shown in Fig. 7a. The results showed these bands reacted with an anti-p-Thr 167 RXRα antibody increased dramatically by fasting in WT mice, while no such increase was observed in RXRα T167A mice. Thus, these data suggested RXRα Thr 167 was phosphorylated after fasting in adipose tissues from WT mice. Thus, observed phosphorylation of RXRα may modulate RXRα activity with its heterodimer partner and alter gene expression in adipose tissue observed in Fig. 5c. Next, we compared canonical lipid metabolism gene expression in adipose tissue between WT and T167A mice. In contrast to the results obtained for the liver shown in Fig. 6b, we observed altered expression of 5 genes among 12 lipid metabolism-related genes in the adipose tissue (Fig. 7b, and Supplemental Fig. 3).

To support the notion that the observed differential gene expression were regulated by RXRα, we utilized a agonist LG100268 to treat WT and $Rxr\alpha^{T167A}$. WT and T167A mice in both fed and fasted conditions. Gene expressions

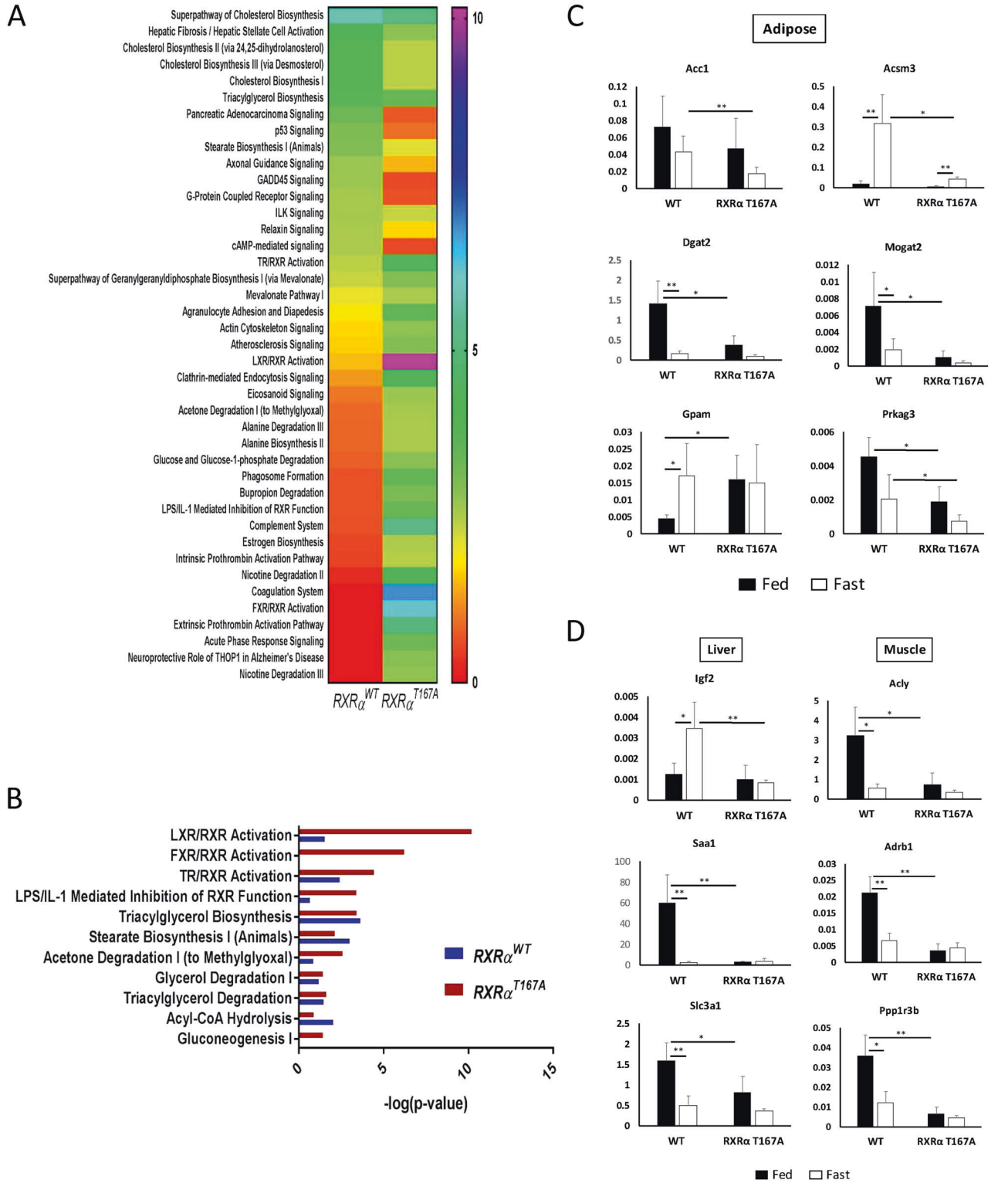

obtained from adipose tissues were shown in Fig. 7c and Supplemental Fig. 4. Three genes, *Scd1*, *Pck1*, and *Mogat2* were clearly affected by single oral administration of LG100268. Of note, these three genes respond to LG100268 in different manners. *Scd1* was activated by exposures to the ligand in WT and T167A mice, except for the fasted WT, in which RXRα T167 phosphorylation was observed. In contrast, *Pck1* was repressed only in the WT-fasted condition. *Mogat2* was activated in WT-fed condition, but no effect was observed in other categories.

◀ **Fig. 5** Canonical pathway analysis of DNA microarray data and confirmed differential gene expression. **a** Canonical pathway analysis was performed with Ingenuity Pathway Analysis as described in Materials and methods. Canonical pathways of which $-\log(P$ value) were >2.5 in either WT or $Rxr\alpha^{T167A}$ were used to produce this heat map. Wild-type (WT) pathways were placed in order of higher to lower $-\log(P$ value)s and compared with those from $Rxr\alpha^{T167A}$ mice. **b** Canonical pathway analysis depends on selected metabolism and RXRα-related pathways. **c** Confirmed differential gene expression in white adipose tissue between WT and $Rxr\alpha^{T167A}$ mice in fed and fasted conditions by quantitative PCR (qPCR) analyses ($n = 4$). Vertical axes indicate the relative amount of mRNA from each gene vs. that of β-actin. Values are means ± SD. $^*P < 0.05$, and $^{**}P < 0.01$. **d** Confirmed differential gene expression in the liver (left) and muscle (right) between WT and $Rxr\alpha^{T167A}$ mice-fed and -fasted condition by qPCR analyses ($n = 4$). Graph formats are the same as **c**

Schematic diagrams of the obtained results regarding energy-metabolizing enzymes and regulators genes in WAT are presented (Fig. 7d). Here, gene expression changes caused by T167A mutation in either fed or fasted conditions of the genes are shown. These genes are involved in fatty acid synthesis from glucose, triglyceride synthesis from fatty acids, fatty acid catabolism, and their regulating factors. In both fed and fasted conditions, most of the genes we found were involved in lipogenic pathways except for *Acsm3* (Fig. 7d).

Discussion

Here we report the results of phosphorylation of hRXRα at Thr 162 in vitro and mutant mice that have the equivalent Thr 167 mutated to Ala. This residue is located within a PKC phosphorylation consensus sequence and was confirmed to be phosphorylated by PKC in vitro using both cell-free and cultured cell models. We presented evidence suggesting that this phosphorylation affects RXRα activity as a gene transcription factor and its localization in the cells. Mutant mice with RXRα T167A show altered energy metabolism gene expression in multiple organs in both fed and fasting conditions. Blood glucose levels decrease in the mutant mice after fasting was attenuated. Overall, these results suggest that RXRα function as a transcription factor is modulated by Thr 167 phosphorylation in its DBD.

Our group found that the nuclear receptor CAR was phosphorylated at Thr 38 in mouse liver and that dephosphorylation of this residue is a key step for CAR nuclear translocation in response to activation by xenobiotics. Subsequently, we have identified conserved sites in the DBDs (Fig. 1a) of multiple nuclear receptors, which are phosphorylated to modulate each respective receptor's function in a distinct manner. Phosphorylated CAR was inactive in reporter assays, unable to bind its DNA response element (NR1 element in Cyp2b10 and CYP2B6), and

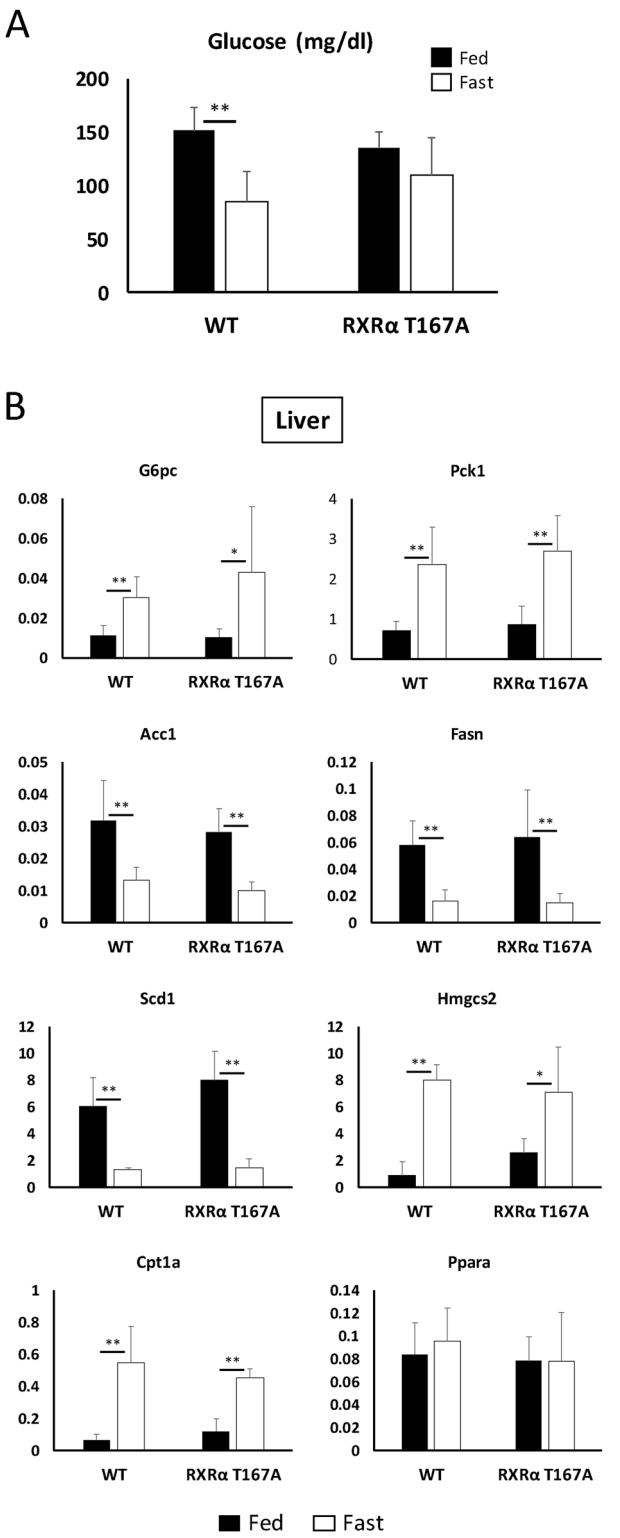

Fig. 6 Blood glucose change and hepatic energy metabolism genes. **a** Blood glucose levels in WT and $Rxr\alpha^{T167A}$ mice in fed and fasted conditions ($n = 6$). $^{**}P < 0.01$. **b** Energy metabolism-related gene expression in the liver determined by quantitative PCR (qPCR) ($n = 4$). Vertical axes indicate the relative amount of messenger RNA (mRNA) from each gene vs. that of β-actin. Values are means ± SD. $^*P < 0.05$, $^{**}P < 0.01$

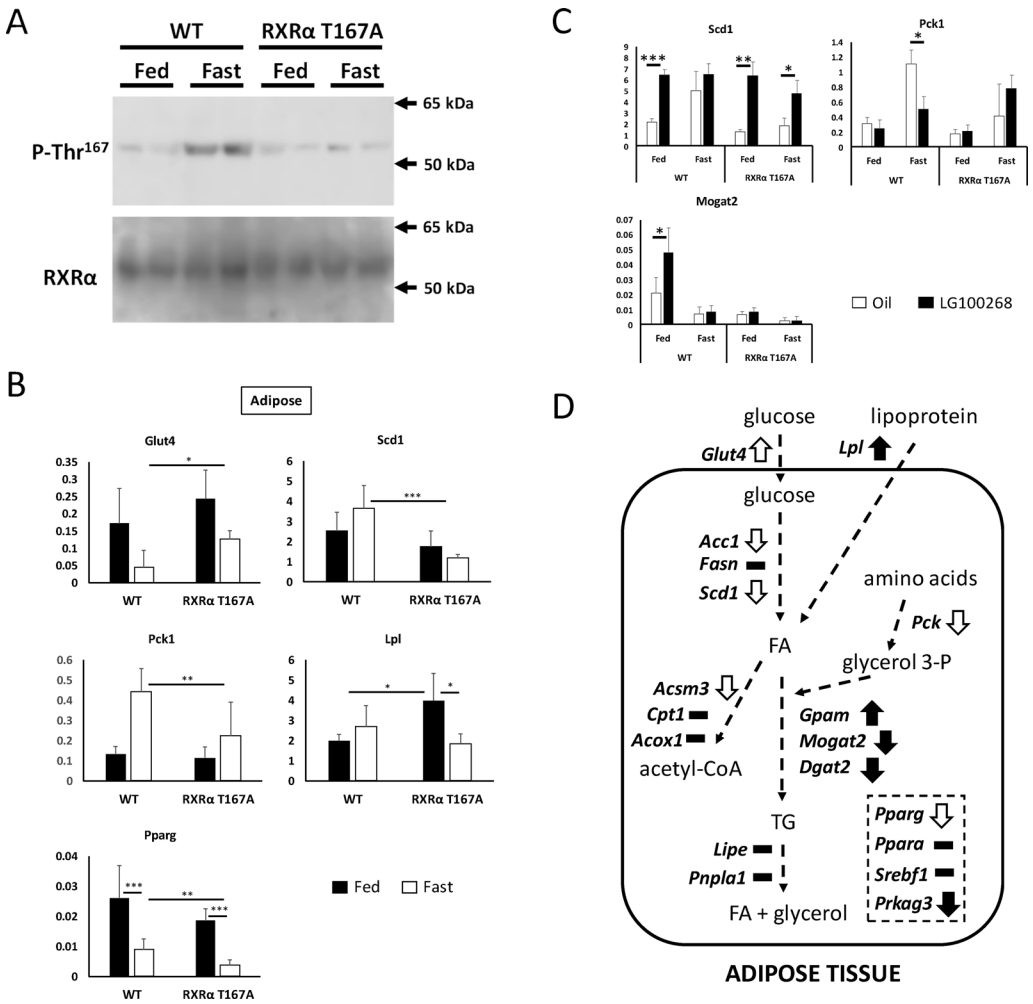

Fig. 7 Gene expression changes in *Rxrα*^{T167A} mice white adipose tissue. **a** Retinoid X receptor α (RXRα) T167 phosphorylation in white adipose tissue. Protein was extracted from adipose tissue and western blotting was performed using anti-p-Thr 167 RXRα antibody as described in Materials and methods section. **b** Lipid metabolism-related gene expression in white adipose tissue determined by quantitative PCR (qPCR) ($n = 4$). Vertical axes indicate the relative amount of messenger RNA (mRNA) from each gene vs. that of β-actin. Values are means ± SD. $^{*}P < 0.05$, $^{**}P < 0.01$, and $^{***}P < 0.001$. **c** Genes in adipose tissue of which expression were affected by RXRα ligand treatment. Genes differentially regulated between wild-type (WT) and T167A knock-in (KI) mice were analyzed with or without RXRα ligand LG100268 single oral dosage ($n = 4$). Vertical axes indicate relative mRNA amount of each gene vs. that of β-actin. Values are means ± SD. $^{*}P < 0.05$, $^{**}P < 0.01$, $^{***}P < 0.001$. **d** Summary of gene expression changes between WT and *Rxrα*^{T167A} mice in adipose tissue of fed and fasted conditions. White and black arrows show changes in fasting and fed conditions, respectively. Solid bar indicates no significant changes observed by T167A mutation. Genes in the dotted line square are regulatory factors, while genes next to the dotted arrows indicate genes that encode the enzymes for these pathways

dysfunctional in its nuclear accumulation after activation [1]. In contrast, phosphorylation of ERα Ser 212 (Fig. 1a) did not compromise ERα activity in gene reporter assays, and a gene array study suggested that a distinct set of genes are activated by the phospho-mimic S212D ERα mutant, compared to S212A ERα [24]. A phospho-specific antibody developed to specifically detect this Ser phosphorylation of ERα found positive staining in peripheral blood neutrophils, and detected migration and infiltration of these cells to the mouse uterus [5, 6]. In the case of FXR, Ser 154 phosphorylation makes this transcription factor inactive for gene reporter assays and unstable, resulting in rapid degradation [4]. Immunohistochemistry with a phospho-specific antibody revealed that FXR was phosphorylated in the nucleus of centrilobular hepatocytes only in ligand-treated mice. The results in this report suggest RXRα T162 phosphorylation gives RXRα divergent function from its non-phosphorylated form. These results all suggest that phosphorylation at the conserved site within their DBDs is critically regulating receptor function. Some of the alterations brought by phosphorylation appear to be specific to each receptor, and others are common to multiple receptors. In a recent publication about the hepatocyte nuclear factor 4α complex with its DNA response element and

coactivator-derived peptides, the authors showed Thr 78, which is the homologous residue to Thr 167 of RXRα, physically bridges the DBD to the ligand-binding domain (LBD) [25]. They suggested phosphorylation of this residue may compromise the integrity of the quaternary fold needed for efficient DNA binding [26]. How this information can be applicable to other nuclear receptors is not clear at this point. Nonetheless, the very limited knowledge about the molecular mechanism of phosphorylation and receptor function makes further detailed discussion a speculative exercise at this juncture. Future studies about this conserved phosphorylation site in nuclear receptors, including the receptors described here with detailed molecular mechanistic and structural analysis will be necessary.

Phosphorylation of multiple sites in the RXRα molecule and the biological functions of these phosphorylation states have been studied in many publications [12, 27–29]. Earlier studies identified four residues in the AF1 domain (Ser 22, Ser61, Ser75, and Thr87) and one in the LBD (Ser 265). Stress kinase c-Jun N-terminal kinase was found to phosphorylate Ser 265 and modulate RXRα activity [27]. Utilizing a RXRα-null cell line and mutant RXRα expressed in the cell background, RXRα activity alteration by phosphorylation was found to be promoter dependent. Furthermore, a recent report found that Ser 260 phosphorylation in human RXRα impairs the receptor's subcellular localization, receptor interaction, nuclear mobility and vitamin D-dependent DNA binding in keratinocytes [13]. Regarding Thr 162 phosphorylation in DBD, Sun et al. found PKC phosphorylates this site in vitro using bacterially expressed RXRα DBD [8]. They found intracellular localization changes with the phospho-mimic mutant of GFP-RXRα in Cos-7 cells. However, the functional effect of this phosphorylation on RXRα was not known until this report. The results in this paper demonstrate phosphorylation of the Thr residue (within the DBD of RXRα) in vivo (Fig. 7a), and gene reporter assays suggest RXRα activity modulation is promoter dependent, as shown in Fig. 1c. Gel shift assay and gene reporter assay (Fig. 1b, c) results suggest that phosphorylation at this residue may have diverse effect on RXRα activity depending on which heterodimer partner is in action. Moreover, YFP-RXRα localization in the liver was affected by phospho-mimetic mutation of Thr 162 (Fig. 2c–e). There appears to be similar effects for Thr 162 and Ser 260 phosphorylation on RXRα. Both yielded promoter-dependent effects on its activity as a transcription factor and affected its subcellular localization. The fundamental purpose of these phosphorylation events, one in DBD and the other in LBD, to cause similar effects on RXRα activity remains an open question. Moreover, possible regulation of RXRα activity by Thr 167 phosphorylation in combination with other phosphorylation sites may become an interesting research target.

We had tried to develop mice with Thr 167 mutated to Asp; however, all homozygote mutant mice died before birth (data not shown). The model mice in this report (with the same Thr mutated to Ala) showed no apparent phenotype, as long as the mice were fed normally. The findings that T167D RXRα exhibited higher activity than T167A RXRα in PPARγ gene reporter assays, while a reversed relationship was observed in PPARα reporter assays (Fig. 1c), prompted us to focus on energy metabolism associated genes in mice, many of which are PPAR target genes. We compared mRNA expression in the adipose, liver, and muscle between WT and mutant mice using microarray analysis. We then examined the affected canonical pathways of glucose and lipid metabolism in these organs. Our data clearly show that mutant mice had very different gene expression profiles in key enzymes of the energy metabolism system in multiple organs in both fed and fasted conditions (Figs. 4–7, Table 1, Supplement Tables 1–3). Furthermore, we observed that RXRα Thr 167 phosphorylation was increased by fasting in adipose tissue (Fig. 7a) using a Thr 167 phospho-specific antibody, while $Rxr\alpha^{T167A}$ mice did not show this increase of phosphorylated RXRα as expected. Results shown in Fig. 1c with phosphorylation-mimicking mutant T162D and phospho-deficient mutant T162A suggested that phosphorylation increases RXRα activity when partnered with PPARγ and decreases its activity when partnered with PPARα or CAR. Thus, the transcriptional activity of RXRα with multiple partners including PPARγ is supposed to be different between WT and $Rxr\alpha^{T167A}$ mice adipose tissue when mice are fasted. Those expected diverse effect of the Thr 167 phosphorylation may explain some of the observed gene expression differences between WT and $Rxr\alpha^{T167A}$ mice. Although our knowledge about the phosphorylation in vivo is limited at this point, this phosphorylation is possibly happening in many tissues with unidentified stimuli and diversifying RXRα activity regulation. $Rxr\alpha^{T167A}$ mice have strong potential to serve as a model system to determine RXRα Thr 167 phosphorylation-deficient mutation effects in vivo.

In the adipose tissue of fasted KI mice compared with that of fasted WT mice, *Acc1*, *Scd1*, *Pck1*, *Acsm3*, *Prkag3*, and *Pparg* genes were downregulated, while *Glut4* gene was upregulated (Figs. 5c, 7b, c). In addition, *Fasn*, *Mogat2*, and *Dgat2* were lower, though not statistically significant. Among these, *Acc1*, *Fasn*, and *Scd1* genes produce key enzymes for de novo lipogenesis, while *Gpam*, *Mogat2*, and *Dgat2* are for triglyceride synthesis from fatty acid and glyceraldehyde 3-phosphate. *Pck1* supplies glyceraldehyde 3-phosphate for triglyceride synthesis. *Prkag3* as a AMPK kinase regulatory subunit and *Pparg* as a transcription factor regulate gene expression and protein function associated with energy metabolism. In fasting

condition *Fasn*, a key gene of lipid synthesis, mRNA levels were 10 and 6% of those in fed condition in WT and T167A KI mice, respectively. Thus, fatty acid synthesis from glucose seems to be much lower in fasted mice compared with fed mice as expected. Major glucose supplier in the fasted mice in this report (at 24 h fasting) should be hepatic gluconeogenesis with depleted glycogenolysis in the liver with no food intake [30]. In such limited glucose supply, glucose usage changes caused by lower expression of *Acc1*, *Scd1*, and *Pck1* in adipocytes may explain, at least partially, the compromised glucose level reduction in fasted KI mice compared to fasted WT mice (Figs. 6a, 7d).

Genes involved in lipid metabolism have differential expression in the fed condition. *Lpl*, *Gpam*, *Prakag3*, *Mogat2*, and *Dgat2* in adipose (Figs. 5c, 7b, c) and *Acly* (Fig. 5d) in the muscle had altered expression between WT and KI mice. *Adrb1* in the muscle showed a difference in the fed condition, and was recently reported to be involved in cold- and diet-induced thermogenesis. Interestingly, whole-body knockout of this gene resulted in the mice exhibiting fasting-induced hyperglycemia [31]. Despite these gene expression changes, we observed no difference in the biological parameters between WT and KI mice in the fed condition. How these changes of gene expression are related with the observed minimal changes in biological parameters is currently not elucidated.

Transcriptional mechanisms of altered gene expression in KI mice are unknown. The four observed patterns of gene expression changes between WT and KI (fed, WT > KI; fed, WT < KI; fasted, WT > KI, fasted WT < KI) imply that multiple mechanisms are involved to regulate associated gene expression. Expressions of three genes (*Scd1*, *Pck1*, and *Mogat2*) in mouse adipose were shown to be modulated by single oral dosage of RXR-selective ligand LG100268 (Fig. 7c). Since LG100268 activates RXRα, RXRβ, and RXRγ, it is possible that RXRβ and/or RXRγ were involved in the gene regulation. However, the observed gene expression pattern in Fig. 7c strongly suggested functional interaction between RXRαT167A mutation and LG100268 treatments. Thus, these genes appeared to be directly regulated by heterodimers containing RXRα and T167 phosphorylation affected the expression in gene-specific manner. Since each organ has its own set of RXRα heterodimer partner downstream target genes, possible combinations between phosphorylation status and these partners could regulate gene expression differently between WT and KI mice in an organ-specific manner. Furthermore, indirect regulation through other transcription factors regulated by the RXRα complex and/or perturbation of endocrine systems caused by the lack of RXRα phosphorylation may occur in these mice. In this regard, our results are limited to mice with a normal energy metabolism background compared to fed and fasted conditions. If we continue this study in conjunction with mouse model systems of metabolic diseases, such as obesity and diabetes, or with high fat diet feeding condition, more insight for the observed complex transcriptional alteration in KI mice may be obtained. Information about the functional interaction of RXRα T167 phosphorylation with the canonical energy metabolism signaling system will enable better defined functional relationships in mouse energy metabolism.

Since RXRα is ubiquitously expressed in almost all organs, information regarding the T167 phosphorylation status in each organ/tissue is essential for elucidating the biological functions of T167 phosphorylation. Fasting may affect phosphorylation differently in other organs distinct from the relationships observed in this study. Aside from fasting, other stimuli in each organ/tissue may cause phosphorylation/dephosphorylation through unidentified signaling systems with various sets of pathway-specific kinases and phosphatases. Nonetheless, our knowledge about these mutant mice is very limited at this point, and T167A mutant mice will be a useful model system to study the biological functions of RXRα phosphorylation.

Acknowledgements We thank the fluorescence microscopy and imaging center, knockout mouse core laboratory, molecular genomics core laboratory, and DNA sequence core laboratory of NIEHS and Dr. Frank Gonzalez, NCI, NIH. This work was supported by National Institutes of Health intramural research program Z01ES1005-01.

Compliance with ethical standards

Conflict of interest The authors declare that they have no conflict of interest.

References

1. Mutoh S, Osabe M, Inoue K, Moore R, Pedersen L, Perera L, et al. Dephosphorylation of threonine 38 is required for nuclear translocation and activation of human xenobiotic receptor CAR (NR1I3). J Biol Chem. 2009;284:34785–92.
2. Mutoh S, Sobhany M, Moore R, Perera L, Pedersen L, Sueyoshi T, et al. Phenobarbital indirectly activates the constitutive active androstane receptor (CAR) by inhibition of epidermal growth factor receptor signaling. Sci Signal. 2013;6:ra31.
3. Hori T, Moore R, Negishi M. p38 MAP kinase links CAR activation and inactivation in the nucleus via phosphorylation at threonine 38. Drug Metab Dispos. 2016;44:871–6.
4. Hashiguchi T, Arakawa S, Takahashi S, Gonzalez FJ, Sueyoshi T, Negishi M. Phosphorylation of farnesoid X receptor at serine 154 links ligand activation with degradation. Mol Endocrinol. 2016;30:1070–80.
5. Shindo S, Moore R, Flake G, Negishi M. Serine 216 phosphorylation of estrogen receptor alpha in neutrophils: migration and infiltration into the mouse uterus. PLoS ONE. 2013;8:e84462.
6. Shindo S, Moore R, Negishi M. Detection and functional analysis of estrogen receptor alpha phosphorylated at serine 216 in mouse neutrophils. Methods Mol Biol. 2016;1366:413–24.

7. Hsieh JC, Jurutka PW, Galligan MA, Terpening CM, Haussler CA, Samuels DS, et al. Human vitamin D receptor is selectively phosphorylated by protein kinase C on serine 51, a residue crucial to its trans-activation function. Proc Natl Acad Sci USA. 1991;88:9315–9.
8. Sun K, Montana V, Chellappa K, Brelivet Y, Moras D, Maeda Y, et al. Phosphorylation of a conserved serine in the deoxyribonucleic acid binding domain of nuclear receptors alters intracellular localization. Mol Endocrinol. 2007;21:1297–311.
9. Germain P, Chambon P, Eichele G, Evans RM, Lazar MA, Leid M, et al. International Union of Pharmacology. LXIII. Retinoid X receptors. Pharmacol Rev. 2006;58:760–72.
10. Lefebvre P, Benomar Y, Staels B. Retinoid X receptors: common heterodimerization partners with distinct functions. Trends Endocrinol Metab. 2010;21:676–83.
11. Evans RM, Mangelsdorf DJ. Nuclear receptors, RXR, and the Big Bang. Cell. 2014;157:255–66.
12. Dawson MI, Xia Z. The retinoid X receptors and their ligands. Biochim Biophys Acta. 2012;1821:21–56.
13. Jusu S, Presley JF, Kremer R. Phosphorylation of human retinoid X receptor alpha at serine 260 impairs its subcellular localization, receptor interaction, nuclear mobility, and 1alpha,25-dihydroxyvitamin D3-dependent DNA binding in Ras-transformed keratinocytes. J Biol Chem. 2017;292:1490–509.
14. Yeung EY, Sueyoshi T, Negishi M, Chang TK. Identification of *Ginkgo biloba* as a novel activator of pregnane X receptor. Drug Metab Dispos. 2008;36:2270–6.
15. Kawamoto T, Sueyoshi T, Zelko I, Moore R, Washburn K, Negishi M. Phenobarbital-responsive nuclear translocation of the receptor CAR in induction of the CYP2B gene. Mol Cell Biol. 1999;19:6318–22.
16. Sueyoshi T, Kawamoto T, Zelko I, Honkakoski P, Negishi M. The repressed nuclear receptor CAR responds to phenobarbital in activating the human CYP2B6 gene. J Biol Chem. 1999;274:6043–6.
17. Matsusue K, Miyoshi A, Yamano S, Gonzalez FJ. Ligand-activated PPARbeta efficiently represses the induction of LXR-dependent promoter activity through competition with RXR. Mol Cell Endocrinol. 2006;256:23–33.
18. Soh JW, Weinstein IB. Roles of specific isoforms of protein kinase C in the transcriptional control of cyclin D1 and related genes. J Biol Chem. 2003;278:34709–16.
19. Honkakoski P, Zelko I, Sueyoshi T, Negishi M. The nuclear orphan receptor CAR-retinoid X receptor heterodimer activates the phenobarbital-responsive enhancer module of the CYP2B gene. Mol Cell Biol. 1998;18:5652–8.
20. Juge-Aubry C, Pernin A, Favez T, Burger AG, Wahli W, Meier CA, et al. DNA binding properties of peroxisome proliferator-activated receptor subtypes on various natural peroxisome proliferator response elements. Importance of the 5'-flanking region. J Biol Chem. 1997;272:25252–9.
21. Konno Y, Kodama S, Moore R, Kamiya N, Negishi M. Nuclear xenobiotic receptor pregnane X receptor locks corepressor silencing mediator for retinoid and thyroid hormone receptors (SMRT) onto the CYP24A1 promoter to attenuate vitamin D3 activation. Mol Pharmacol. 2009;75:265–71.
22. Kodama S, Negishi M. Pregnane X receptor PXR activates the GADD45beta gene, eliciting the p38 MAPK signal and cell migration. J Biol Chem. 2011;286:3570–8.
23. Sajic T, Hopfgartner G, Szanto I, Varesio E. Comparison of three detergent-free protein extraction protocols for white adipose tissue. Anal Biochem. 2011;415:215–7.
24. Shindo S, Sakuma T, Negishi M, Squires J. Phosphorylation of serine 212 confers novel activity to human estrogen receptor alpha. Steroids. 2012;77:448–53.
25. Chandra V, Huang P, Potluri N, Wu D, Kim Y, Rastinejad F. Multidomain integration in the structure of the HNF-4alpha nuclear receptor complex. Nature. 2013;495:394–8.
26. Rastinejad F, Ollendorff V, Polikarpov I. Nuclear receptor full-length architectures: confronting myth and illusion with high resolution. Trends Biochem Sci. 2015;40:16–24.
27. Bruck N, Bastien J, Bour G, Tarrade A, Plassat JL, Bauer A, et al. Phosphorylation of the retinoid x receptor at the omega loop, modulates the expression of retinoic-acid-target genes with a promoter context specificity. Cell Signal. 2005;17:1229–39.
28. Bastien J, Rochette-Egly C. Nuclear retinoid receptors and the transcription of retinoid-target genes. Gene. 2004;328:1–16.
29. Bastien J, Adam-Stitah S, Plassat JL, Chambon P, Rochette-Egly C. The phosphorylation site located in the A region of retinoic X receptor alpha is required for the antiproliferative effect of retinoic acid (RA) and the activation of RA target genes in F9 cells. J Biol Chem. 2002;277:28683–9.
30. Jensen TL, Kiersgaard MK, Sorensen DB, Mikkelsen LF. Fasting of mice: a review. Lab Anim. 2013;47:225–40.
31. Ueta CB, Fernandes GW, Capelo LP, Fonseca TL, Maculan FD, Gouveia CH, et al. Beta(1) adrenergic receptor is key to cold- and diet-induced thermogenesis in mice. J Endocrinol. 2012; 214:359–65.